Noname manuscript No.
(will be inserted by the editor)

Deorbiter CubeSat Mission Design

Houman Hakima · M. Reza Emami

Received: date / Accepted: date

Abstract This paper discusses the design concept and operations of an active debris removal mission intended for the removal of sizable debris objects from low Earth orbit. The mission consists of a spacecraft that carries and deploys several debris-removing CubeSats, called deorbiter. The CubeSats are designed based on the utilization of eight-unit form factor and commercially available components with significant flight heritage. Upon release from the mothership, each deorbiter proceeds to performing a rendezvous and attachment maneuver with a pre-determined debris object. Once attached to the debris, the CubeSat performs a detumbling maneuver, by which the residual angular momentum of the debris is dumped using CubeSat onboard reaction wheels. After stabilizing the debris attitude, the CubeSat proceeds to performing a deorbiting maneuver, i.e., reducing the debris altitude where it disintegrates and burns up due to atmospheric drag, typically at around 100 km above Earth. Several aspects of the mission are described, including the mothership and deorbiter CubeSat. The target debris objects to be removed in the mission are selected using a systematic approach, based on several factors, including the orbit of resident objects and their collision probabilities, as well as the physical parameters of the objects, e.g., shape, size, and mass. The attitude and orbital maneuvers that are planned for the mission are described, and the performance of the deorbiter CubeSat during each operation is investigated. Using the actual performance parameters of the CubeSat onboard components, each maneuver is simulated in MATLAB, and performance of the deorbiter CubeSat is discussed in light of the simulation results.

Keywords Active debris removal · Mission design · Debris selection · Deorbiter CubeSat

Houman Hakima
Ph.D. Candidate, Institute for Aerospace Studies, University of Toronto, Canada
E-mail: houman.hakima@utoronto.ca

M. Reza Emami
Director, Space Mechatronics Group, University of Toronto Canada
E-mail: reza.emami@utoronto.ca

1 Introduction

The current environment of man-made intact and debris objects in space is a mirror image of more than half a century of space activities, following the launch of Sputnik-1 on Oct. 4, 1957. Space activities have left traces behind, in the form of what is known as *space debris*. The Inter-Agency Space Debris Coordination Committee (IADC) formally defines space debris as all man-made objects, including fragments, in Earth orbit or re-entering the atmosphere, which are non functional [1]. They include defunct satellites and spent rocket stages, as well as the fragments from their disintegration and collisions. To date, there have been about 5,300 successful satellite launches [2], and certain orbits, such as the low Earth orbit (LEO), are at risk of becoming congested.

Space debris pose serious threats to the safety of astronauts and humans on Earth, as well as to the well-being of space assets, e.g., the International Space Station. As such, there has been a keen interest in the space community in the development of novel remediation and mitigation techniques for space debris environment. Some of the most-studied active debris removal methods include robotic arms [3,4], nets and harpoons [5,6], electrodynamic tether [7,8], ion beam shepherd [9,10], and ground/space-based laser systems [11,12]. More recently, a CubeSat-based concept was proposed in [13], which is intended for the removal of sizable debris objects from LEO. The spacecraft, called the deorbiter CubeSat, utilizes an eight-unit (8U) form factor and commercially available components with considerable space heritage, and has an overall mass of 16.0 kg. Several deorbiters may be carried into orbit onboard a carrier spacecraft known as mothership, allowing for the removal of several debris objects in a single mission.

The organization of this paper is as follows: An overview of the deorbiter CubeSat mission concept is presented in Section 2. The engineering design of the deorbiter CubeSat is described in Section 3. A discussion of the target debris selection methodology is presented in Section 4. Orbital and attitude control maneuvers that are planned for the mission are discussed in Section 5. Concluding remarks are presented in Section 6.

2 Deorbiter CubeSat mission

In the proposed ADR mission, debris removal is carried out by a deorbiter CubeSat. Each CubeSat is intended for the removal of one debris object, and so a mothership may carry and deploy multiple of such CubeSats into orbit if multiple debris objects are to be removed in a mission. After separation from the launch vehicle, the mothership (shown in Fig. 1) acquires a relative parking orbit of a few kilometres relative to the (first) target debris. From there, the mothership begins to estimate the attitude and orbital state of the debris using its onboard optical sensors and computer vision algorithms, as described in the literature (e.g., [14]). Once an initial estimate of the debris state is obtained and transferred to a deorbiter CubeSat, the mothership deploys the CubeSat. To prepare for the rendezvous and attachment maneuvers, the CubeSat first deploys its solar panels and activates the onboard avionics, transitioning from the stowed configuration to the deployed configuration. Then, the CubeSat is navigated towards the target debris, through the control commands transmitted from the mothership. In this mission, the concurrent orbital

and attitude control commands for the CubeSat to synchronize and rendezvous with the debris (see, e.g., [15]) are computed onboard the mothership, due to its higher computational and measurement capabilities, and transmitted to the CubeSat for controlling its position and attitude. The CubeSat also needs to send the mothership, via an inersatellite link, the information about its instantaneous attitude for control computations. Upon completion of the CubeSat's rendezvous with the debris and attachment, the mothership will move on to the next debris. The process of stabilizing the debris rotational motion begins, which is achieved through using the onboard attitude determination sensors and control actuators. Once the debris is successfully detumbled, the CubeSat begins a deorbiting operation using the onboard low-thrust propulsion system. Since the amount of available propellant is highly restricted on the deorbiter CubeSat, any plane change maneuver is avoided, and the initial, intermediate and final orbits are assumed to be co-planar. The deorbitation is achieved by reducing the debris orbital height to 100 km, where atmospheric density and the resulting drag are sufficiently high for disintegrating and burning up the debris.

In terms of the mission timeline, previous studies have shown that the detumbling operation can be accomplished within a few days, while the deorbiting is achieved within five years, considering sub-1000 kg debris objects in LEO [13], which is significantly shorter than the natural lifetime of resident objects in LEO. Figure 2 shows the approximate lifetime of LEO objects with area (A) to mass (M) ratio of $A/m = 0.5\ \mathrm{m}^2/\mathrm{kg}$ (dashed lines) and $A/m = 2.0\ \mathrm{m}^2/\mathrm{kg}$ (solid lines). The atmospheric density is estimated using the Harris-Priester model [16, pg. 513], which is a table look-up model presenting the minimum and maximum atmospheric density values (depending on the solar activity level), $\rho_{\mathrm{a,min}}$ and $\rho_{\mathrm{a,max}}$, respectively, for various altitudes. In the figure, $\rho_{\mathrm{a,avg}}$ refers to the average atmospheric density, $\rho_{\mathrm{a,avg}} = \left(\rho_{\mathrm{a,min}} + \rho_{\mathrm{a,max}}\right)/2$.

3 Deorbiter CubeSat design

Figure 3 shows an exploded view of a deorbiter CubeSat, which measures roughly 23 cm to a side in the stowed configuration, and 25 cm × 66 cm × 66 cm (along the x, y, and z axes, respectively) in the deployed configuration, with an overall mass of 16.0 kg. Component selection for the spacecraft is mainly inspired by mission scenarios, availability of the components, and their flight heritage and technology readiness level (TRL). The overall components cost for each deorbiter is estimated

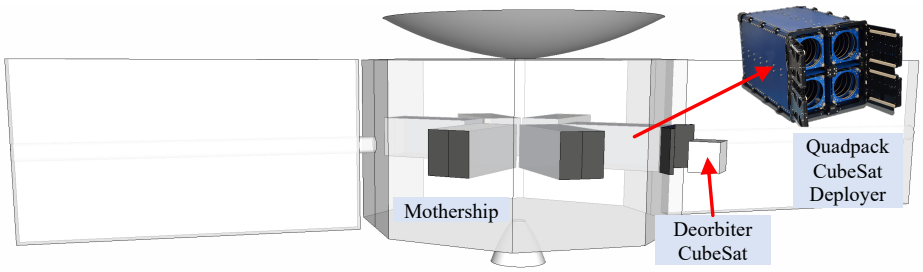

Fig. 1 A preliminary concept for the mothership spacecraft.

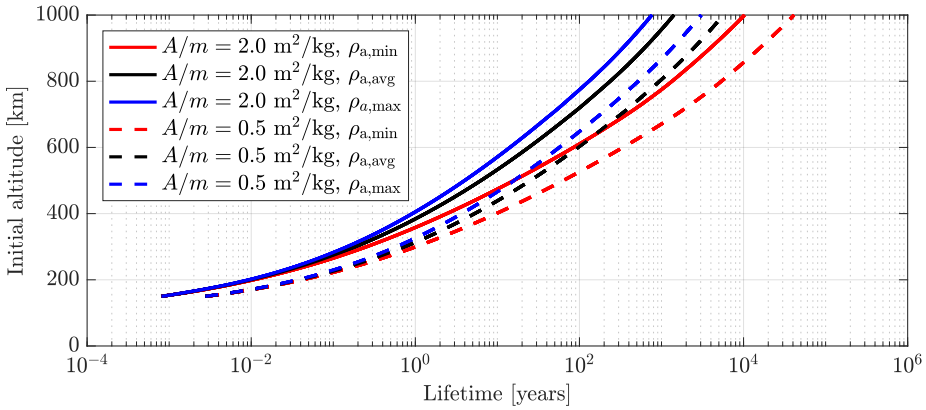

Fig. 2 Expected lifetime of space debris objects.

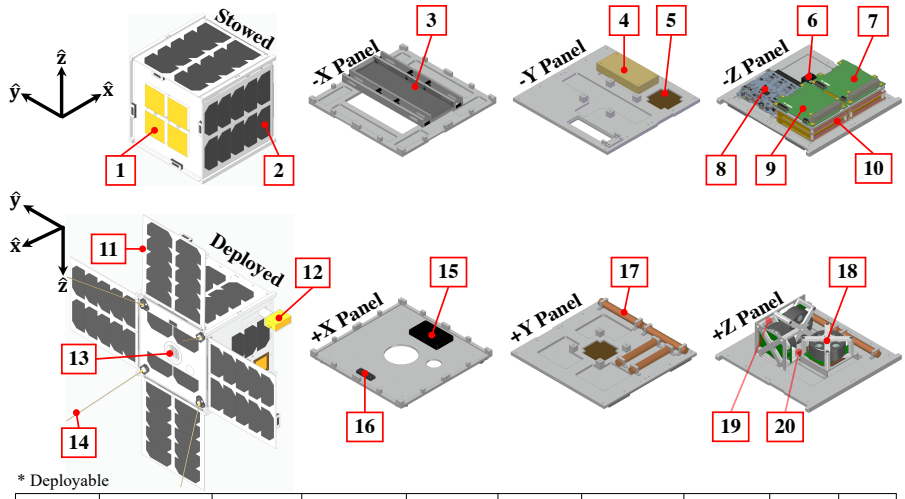

* Deployable

1	2	3	4	5	6	7	8	9	10
Sticky pad* (×4)	Solar Cell (×64)	Attachment mechanism	S-band transmitter	S-band antenna (×2)	Rate sensor	Housekeeping computer	Power board	Attitude computer	Battery (×4)
11	**12**	**13**	**14**	**15**	**16**	**17**	**18**	**19**	**20**
Solar panel* (×4)	Magnetometer*	RF ion thruster	UHF antenna* (×4)	UHF Radio Receiver	Sun sensor (×5)	Magnetorquer (×6)	Reaction wheels (×3)	GPS receiver	GPS antenna

Fig. 3 A snapshot of the deorbiter CubeSat engineering model and the constituting components.

at about $500,000 US [13]. The CubeSat is mainly composed of commercial-off-the-shelf components, which are detailed in [13,17]. In particular, a rate sensor, five sun sensors, and a three-axis magnetometer are embedded on the spacecraft, allowing for attitude determination throughout the orbit. For attitude control, the CubeSat is equipped with three reaction wheels that are mounted in a mutually-perpendicular configuration (see *item 18* in Fig. 3). Further, magnetorquers are used for reaction wheels desaturation. The geometry of magnetorquers is constrained by the spacecraft mechanical design. As such, instead of using three long rods, six

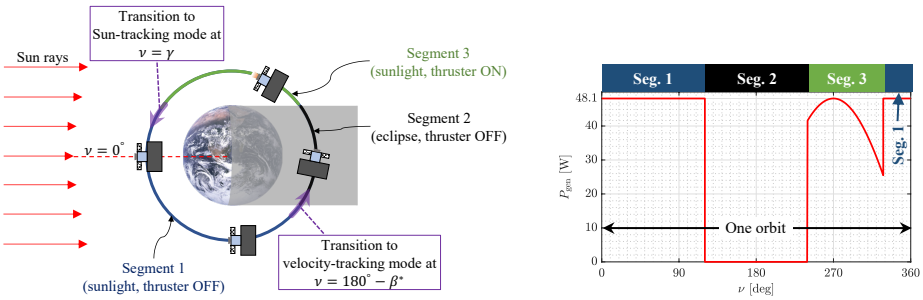

Fig. 4 Left: A nominal operations scenario; Right: Power generated during the nominal scenario. ν denotes the spacecraft angular position in orbit and $0^\circ \leq \beta^* \leq 90^\circ$ is the angle at which the eclipse begins.

shorter rods are combined in pairs to produce a magnetic dipole moment along each principal axis of the spacecraft.

For orbit determination, the spacecraft includes a global navigation system (GPS) sensor, and for orbit control, an electric propulsion system (radio frequency ion thruster) is included. The thruster is utilized by the deorbiter both during the rendezvous and attachment maneuver (after separation from the mothership), as well as during the deorbiting maneuver (while attached to the debris). For the deorbiter CubeSat, Busek Ion Thruster-3 cm (BIT-3) is the propulsion system of choice (TRL 5), which has also been selected by NASA for two upcoming small spacecraft missions, namely, IceCube and LunaH-Map, both planned for launch in 2020 [18]. The main reason behind selecting BIT-3 is that the thruster utilizes iodine as propellant, while most other miniaturized thrusters use xenon [19]. Iodine is more attractive than xenon since (a) it can be stored in solid state at room temperature and has a very low storage pressure, allowing for constructing the propellant tank out of lightweight materials such as plastic [18], and (b) the cost of iodine is about one-fifth of xenon [18]. BIT-3 can provide a maximum thrust and specific impulse of 1.2 mN and 2300 s, respectively, while consuming between 56–89 W of power. Through the systems engineering of the deorbiter CubeSat, it has been determined that the spacecraft can carry up to 6.0 kg of solid iodine in a mission. Hence, the propulsion system would occupy about 2.3U of the 8U form factor.

The main components of the deorbiter's power subsystem are 62 solar cells (30% efficiency [20]), four batteries (each containing eight 7-mm-thick Li-poly cells [21]), wiring harnesses, and a power board that has power converters and battery charge/discharge regulators [22]. There are four deployable solar panels that are articulated only after the deorbiter leaves the deployment canister (QuadPack deployer [23]) inside the mothership, which can generate a maximum electrical energy of 48.1 W·h in the Sun-tracking mode. The battery banks onboard the CubeSat can provide, in total, 29.6 V of voltage and 212.8 W·h of electrical energy, at 7.2 A·h of current capacity. After performing a power budget analysis, it was determined that the deorbiter can operate the thruster (the highest power-consuming component) for about 35% of an orbit, while there are no significant restrictions on the operations of other components. Figure 4 shows a nominal operations scenario and the amount of power generated in the orbit.

Lastly, in terms of the communications subsystem, a S-band radio (a transmitter and two patch antennas) is used by the deorbiter for downlink communications, as well as establishing an intersatellite link with the mothership. A UHF radio (a receiver and four canted monopole antennas) is used to receive uplink data. For a description of the remaining subsystems, the reader is referred to [13,17].

4 Target debris selection

Depending on the objective of an ADR mission, debris obejects may be prioritize for removal based on several criteria, e.g., remediation of the most crowded regions [24, 25], safety of particular space assets [26,27], or minimum delta-v or time requirements [28,29]. The method adopted by authors in this work is based on the total pairwise collision probability of debris objects (an "all-on-all" assessment method) using the radar cross section (RCS) as well as the two-line elements of objects considered in the analysis. The method is detailed in [30], and the result is summarized in Table 1, where ten debris objects with the highest total collision probability (TCP) values are listed.

Table 1 Debris objects with highest TCP values. (i: Inclination; e: eccentricity; K: Total number of Conjunctions)

No.	NORAD	Name	Launch Year	i [deg]	a [km]	e	RCS [m^2]	K	TCP ($\times 10^{-6}$)
1	19650	SL-16 R/B	1988	71.0	7,218	0.002	11.5130	57	11.5425
2	25407	SL-16 R/B	1998	71.0	7,218	0.001	11.3906	57	11.5425
3	11668	SL-8 R/B	1980	83.0	7,358	0.002	5.2684	58	5.1171
4	4784	SL-8 R/B	1970	74.0	7,354	0.003	4.7108	56	4.9086
5	23659	SL-14 R/B	1995	82.5	7,013	0.003	3.9445	34	2.8736
6	40058	PSLV R/B	2014	98.1	7,013	0.002	5.6947	34	2.8736
7	22006	COSMOS 2195	1992	82.9	7,360	0.004	2.3483	49	2.7729
8	10537	SL-8 R/B	1977	82.9	7,359	0.002	4.2080	48	2.7253
9	8073	SL-8 R/B	1975	82.9	7,357	0.002	4.4940	44	2.4380
10	22487	COSMOS 2233	1993	82.9	7,357	0.004	2.0178	44	2.4380

Firstly it is noted that seven out of ten objects with highest TCP are SL-series launch vehicles (owned by Russia), some of which have been in orbit since 1970s. This is particularly attractive in situations where a single mission is designed for the removal of multiple debris. In this respect, the design of the removal agent can be tailored to the specifications of the SL-series launch vehicles. Secondly, when multiple objects are to be removed, it is highly preferred that the target debris objects have the same inclination (e.g., object No. 3, 5, and 7–10 in Table 1) so as to minimize the amount of delta-v required. Thirdly, the majority ($^7/_{10}$) of the proposed debris objects (listed in Table 1) are within the candidate regions for ADR as proposed by the European Space Agency (ESA) [31]. Five of the proposed objects (No. 3, and 7–10) are within ESA's first proposed region, where the largest number of catastrophic collisions are expected to occur in the next 200 years. Even though the first region is less frequently used today, there are over 300 large (RCS > 1 m^2) objects in this region, which were launched between 1972–2010 and have long orbital lifetime. Another two of the proposed objects (No. 1 and 2) are in the third proposed ESA

region, where currently over 44 large debris with masses over 50 kg exist. Object No. 4 in the table does not quite fit within any ESA candidate regions, however its orbital inclination and altitude are similar to that of those in the third region. Likewise, the orbit of object No. 6 meets the criteria of those in the first ESA proposed region, with the exception that its altitude is about 65 km smaller. The only object that cannot be related to any of the candidate regions is object No. 4 that has an inclination similar to objects both in the first and fifth regions, and an altitude similar to those in the fouth region.

5 Attitude and orbital maneuvers

To accomplish its mission, a deorbiter CubeSat is required to perform several attitude and orbital correction maneuvers. These maneuvers are mainly characterized by mission scenarios, as well as the capabilities and performance of sensors and actuators onboard the spacecraft. A summary of some of the planned maneuvers is presented in this section. For a discussion on the attitude estimation of the deorbiter CubeSat, see [32].

5.1 Redezvous maneuver

As outlined in Section 2, the mothership performs a phasing and a long-range rendezvous manevuers with a target debris to arrive at a parking orbit after separation from the launch vehicle. Then, a deorbiter is deployed, which is required to arrive at the target debris and attach to it. The maneuver is commonly known as the rendezvous and attachment maneuver, and is achieved by using a concurrent attitude and orbit control scheme in the deorbiter CubeSat mission. The controller allows for the simultaneous tracking of debris orientation and orbital by the deorbiter CubeSat through the utilization of onboard ion thruster and reaction wheels. For a detailed discussion of the concurrent attitude and orbit controller, the reader is referred to [15]. It is worth noting that since the deorbiter is equipped with a low thrust propulsion system, there is a restriction on the tumbling rates of target debris. It is determined that the maximum tumbling rates can be in order of $1^\circ/s$ in order to ensure a successful attachment. As noted in [15], a propulsion system capable of providing higher force levels allows for targeting faster-tumbling target debris.

5.2 Detumbling maneuver

After attachment to the target debris, the deorbiter CubeSat must stabilize the debris attitude motion, i.e., nullify its initial angular rates, before proceeding to the deorbiting maneuver that requires pointing of the thruster in a certain direction (discussed in Section 5.3). The attitude dynamics of the CubeSat-debris system is governed by Euler's equations (assuming rigid bodies), as follows:

$$\dot{\boldsymbol{\omega}} = \mathbf{I}^{-1}\left(-\boldsymbol{\omega}^{\times}\mathbf{I}\boldsymbol{\omega} + \boldsymbol{\tau}\right) \tag{1}$$

where $\boldsymbol{\omega}$ denotes the inertial angular velocities, $\mathbf{I}$ denotes the combined CubeSat-debris moments of inertia matrix, and $\boldsymbol{\tau}$ denotes the torques acting on the system,

which contains the control torques, $\boldsymbol{\tau}_c$, provided by the CubeSat, as well as disturbance torques (e.g., gravity gradient torques). Depending on the control objectives, there are several control schemes that can be adopted to achieve detumbling. In this work, the time-optimality of the controller is highly desired since the amount of torques that can be exerted by the reaction wheels system are small. Given the large mass of the target debris, it can take a considerable amount of time for the CubeSat to zero the debris momentum. The time-optimal detumbling controller drives the system from an initial angular velocity, $\boldsymbol{\omega}_0$, to rest in minimum time. Meanwhile, the magnitude of the torque input is restricted to be below the maximum torque τ_w^{max} that each reaction wheel can provide. It can be shown that the optimal control torque $\boldsymbol{\tau}_w^*$ provided by the RWA has the following form [33]:

$$\boldsymbol{\tau}_c^* = \begin{cases} -\dfrac{\mathbf{I}\boldsymbol{\omega}}{\|\mathbf{I}\boldsymbol{\omega}\|}\tau_w^{max} & \text{if } \|\boldsymbol{\omega}\| \geq \sigma \\ \mathbf{0} & \text{otherwise} \end{cases} \tag{2}$$

for an arbitrary small σ below which the system is considered to be detumbled. Figure 5 shows the body rates profiles of a sample target debris object with $\mathbf{I} = \text{diag}\,(325.4, 325.4, 75.1)$ kg·m^2 pertaining to an Orion 50 XL rocket body [13] that has initial angular velocities of $\boldsymbol{\omega}_0 = [1.5 \quad -1.0 \quad -0.5]^T$ rad/s, which results from the execution of the detumbling control law. Evidently, the magnitude of the debris body rate, $\|\boldsymbol{\omega}\|$, continuously decreases from its initial values to zero in about six days, including the time required for reaction wheels desaturation by the magnetorquers. (For a description of the desaturation controller, see [13].)

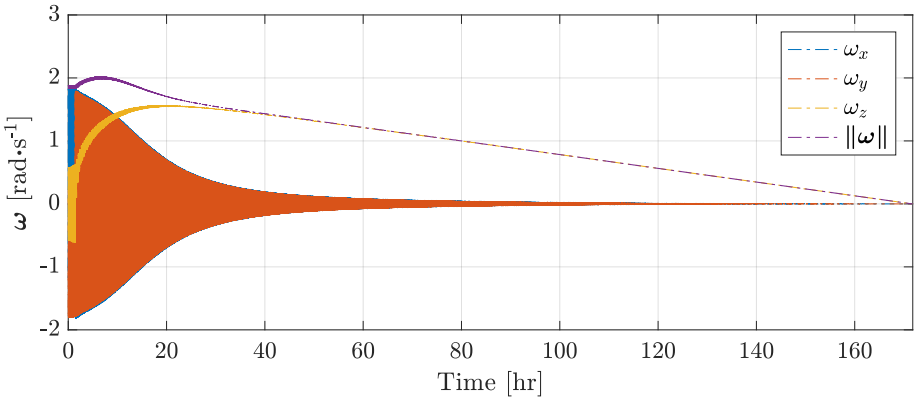

Fig. 5 A sample detumbling maneuver performed by the deorbiter CubeSat.

5.3 Deorbiting maneuver

Deorbiting maneuver is an orbital operation by which the altitude of a target debris is intentionally reduced to about 100-km, where atmospheric drag becomes significant and the debris object disintegrates and burns up. A low-thrust propulsion system, such as an ion engine that has been considered for the deobiter CubeSat,

can provide continuous acceleration (or deceleration) to spacecraft, which can be utilized to gradually modify the shape, size, and orientation of an orbit, as well as the spacecraft's position in the orbit. A common method for modelling the effects of perturbations on the evolution of an orbit is through Gauss' variational equations (GVE) that express the rate of change of the orbital elements. In this work, the non-singular equinoctial elements have been adopted. They are a, i.e., semimajor axis, h_1 and h_2, i.e., the components of the eccentricity vector in the equinoctial frame, p_1 and p_2, i.e., the components of the ascending node vector also in the equinoctial frame, and λ, i.e., the true longitude. Since the objective of the deorbiting maneuver is to reduce the size of a debris orbit, the semimajor-axis component of GVE is of interest in this work[1], defined as follows [34]:

$$\dot{a} = \frac{2a^2}{h}\begin{bmatrix} h_2 \sin\lambda - h_1 \cos\lambda & \dfrac{\ell}{r} & 0 \end{bmatrix}\mathbf{F} \tag{3}$$

where ℓ is the semilatus rectum, h is the magnitude of specific orbital angular momentum (i.e., per unit mass of the spacecraft), r is the radius of orbit, and $\mathbf{F}$ is the total perturbative accelerations expressed in the orbital frame, $\mathcal{F}_{\mathrm{o}}$, defined by the following basis vectors: The x-axis point in the direction of orbital position vector, $\vec{\mathbf{r}}$, the z-axis points along the orbital angular momentum vector, $\vec{\mathbf{h}} = \vec{\mathbf{r}} \times \vec{\mathbf{v}}$, where $\vec{\mathbf{v}}$ denotes the orbital velocity vector, and the y-axis completes the triad (see Fig. 6). The orbital frame is called so since it rotates as the spacecraft progresses in its orbit and hence is non-inertial.

Considering a scenario where the orbital motion of the spacecraft is perturbed by a thrust force, $\mathbf{T}$, and gravitational perturbations, $\mathbf{f}_{J_2}$, the term $\mathbf{F}$ in Eq. (3) can be computed by $\mathbf{F} = \mathbf{T} + \mathbf{f}_{J_2}$. The thrust force, $\mathbf{T}$, can be resolved in $\mathcal{F}_{\mathrm{o}}$ with the help of two steering angles α_1 and α_2, shown in Fig. 6. For a Keplerian orbit, the steering laws corresponding to the fastest rate of decay of semimajor axis, denoted by $\dot{\alpha}_1^{a_{\max}}$ and $\dot{\alpha}_2^{a_{\max}}$, are:

$$\dot{\alpha}_1^{a_{\max}} = \arctan\left(\frac{r\left(h_2 \sin\lambda - h_1 \cos\lambda\right)}{\ell}\right) + \pi \tag{4}$$

$$\dot{\alpha}_2^{a_{\max}} = 0 \tag{5}$$

which is equivalent to exerting a thrust force in the opposite direction of orbital motion.

The gravitational perturbations considered in this study are due to the dominant zonal coefficient, $J_2 \approx 1.0826 \times 10^{-3}$, which is defined in $\mathcal{F}_{\mathrm{o}}$ as follows [35, pg. 262]:

$$\mathbf{f}_{J_2} = \frac{-3\mu_\oplus J_2 R_\oplus^2}{2r^4}\begin{bmatrix} 1 - 12\dfrac{\left(p_2 s_\lambda - p_1 c_\lambda\right)^2}{\left(1 + p_1^2 + p_2^2\right)^2} \\ \dfrac{4\left(p_2 s_\lambda - p_1 c_\lambda\right)\left(p_2 c_\lambda + p_1 s_\lambda\right)}{\left(1 + p_1^2 + p_2^2\right)^2} \\ \dfrac{2\left(p_2 s_\lambda - p_1 c_\lambda\right)\left(1 - p_1^2 - p_2^2\right)}{\left(1 + p_1^2 + p_2^2\right)^2} \end{bmatrix} \tag{6}$$

[1] For a full set of GVE in terms of the equinoctial elements, see [34,35], for instance.

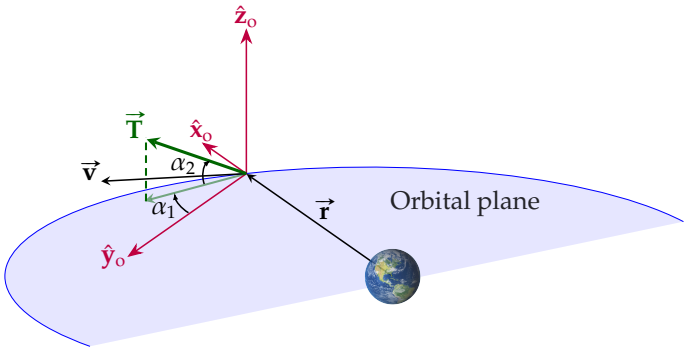

Fig. 6 Definition of the orbital frame, $\mathcal{F}_o$ and steering angles. Angle $-180° \leq \alpha_1 \leq 180°$ is within the plane of orbit, and angle $-90° \leq \alpha_2 \leq 90°$ is out of the plane.

where $\mu_\oplus$ and $R_\oplus$ denote the Earth's standard gravitational parameter and equatorial radius, respectively, and $c_\lambda = \cos\lambda$ and $s_\lambda = \sin\lambda$.

Figure 7 shows debris' semimajor axis profile during the deorbiting maneuvers. Evidently, the semi-major axis is reduced from 7,290 km to 6,478.1 km (denoted by a_f) within 360 days (including contributions from atmospheric drag), which is much shorter than the natural lifetime of the debris (about 20 years [13]). The initial orbital states of the debris object (i.e., Orion 50 XL rocket body with a mass of 366.5 kg [13]) defined in the Earth-centred inertial frame are assumed to be $\mathbf{r} = [3038.4 \quad 412.0 \quad -7069.3]^T$ km and $\mathbf{v} = [-3.71 \quad -5.84 \quad 0.98]^T$ km/s. it is worth noting that the periodic effects of $\mathbf{f}_{J_2}$ on the semimajor axis are evident in Fig. 7, as the semimajor axis values oscillate about a mean value in the short run.

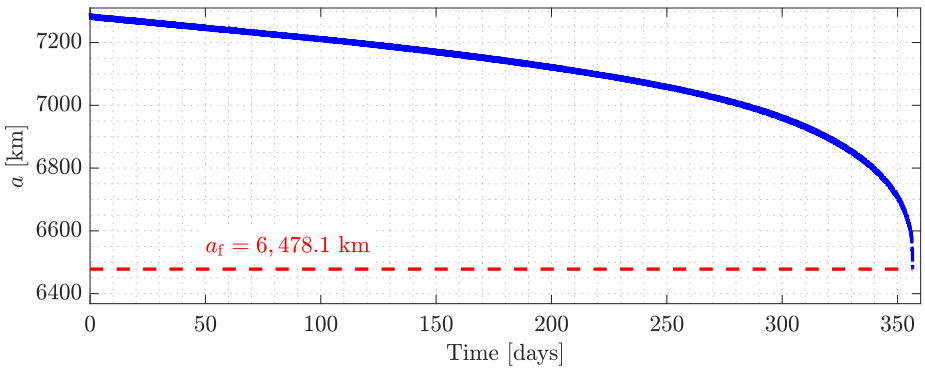

Fig. 7 A sample deorbiting maneuver performed by the deorbiter CubeSat.

6 Conclusion

The mission concept for a deorbiter CubeSat as well as conceptual design of the spacecraft were discussed. The proposed spacecraft is designed based on the utilization of 8U form factor and commercially-available components, and in compliance with the specifications stipulated by the Quadpack deployer dispensing mechanism. An overview of the attitude determination and control, power, and communications subsystems was presented. Several orbital and attitude maneuvers that have been planned for the deorbiter were described, namely, the rendezvous maneuver, detumbling operations, and deorbiting maneuver. The CubeSat uses a low-thrust propulsion system, which is employed during the rendezvous and attachment maneuver, as well as during the deorbiting maneuver, to reduce the debris orbit size over the course of a few years. Numerical simulations were developed in order to investigate the performance of the deorbiter CubeSat in each maneuver, given the performance parameters of the onboard sensors, actuators, and avionics. It was shown that the CubeSat is capable of stabilizing the debris attitude and reducing its orbital lifetime from several decades to a few years, making it a viable solution for near-future debris environment remediation efforts.

References

1. Inter-Agency Space Debris Coordination Committee, IADC space debris mitigation guidelines, IADC-02-01 Rev. 1. Tech. rep. (2007)
2. Union of Concerned Scientists. UCS satellite database. `http://www.ucsusa.org/nuclear-weapons/space-weapons/satellite-database#.V64Z8WXMxSV`. Accessed: 2019-02-15
3. G. Hirzinger, et al., Advanced Robotics **18**(2), 139 (2004). DOI 10.1163/156855304322758006
4. S. Nishida, T. Yoshikawa, in *2008 IEEE International Conference on Robotics and Biomimetics* (2009), pp. 1348–1353. DOI 10.1109/ROBIO.2009.4913196
5. R. Benvenuto, R. Carta, in *Proc. 9th Pegasus-AIAA Student Conference* (American Institute of Aeronautics and Astronautics, 2013)
6. J. Forshaw, Acta Astronautica **127**, 448 (2016)
7. R. Forward, R. Hoyt, in *Proc. 34th AIAA/ASME/SAE/ASEE Joint Propulsion Conference and Exhibit* (American Institute of Aeronautics and Astronautics, 1999)
8. C. Pardini, T. Hanada, P.H. Krisko, Acta Astronautica **64**(5–6), 571 (2009). DOI 10.1016/j.actaastro.2008.10.007
9. S. Kitamura, Y. Hayakawa, S. Kawamoto, Acta Astronautica **94**(2), 725 (2014). DOI 10.1016/j.actaastro.2013.07.037
10. C. Bombardelli, J. Peláez, Journal of Guidance, Control, and Dynamics **34**(3), 916 (2011). DOI 10.2514/1.51832
11. C.R. Phipps, Acta Astronautica **104**(1), 243 (2014). DOI 10.1016/j.actaastro.2014.08.007
12. S. Shen, X. Jin, C. Hao, Chinese Journal of Aeronautics **27**(4), 805 (2014)
13. H. Hakima, M.C.F. Bazzocchi, M.R. Emami, Advances in Space Research **61**(9), 2377 (2018). DOI 10.1016/j.asr.2018.02.021
14. Q. Feng, Z.H. Zhu, Q. Pan, Y. Liu, Advances in Space Research **62**(2), 359 (2018). DOI 10.1016/j.asr.2018.04.034
15. V. Muralidharan, M.R. Emami, Acta Astronautica **138**, 28 (2017). DOI 10.1016/j.actaastro.2017.05.003. The Fifth International Conference on Tethers in Space
16. D.A. Vallado, *Fundamentals of Astrodynamics and Applications*, 1st edn. (McGraw-Hill, 1997)
17. H. Hakima, M.R. Emami, in *Proc. 68th International Astronautical Congress (IAC)* (2017)
18. M. Tsay, et al., in *AIAA/USU Conference on Small Satellites* (Logan, Utah, 2015)
19. NASA. State of the art of small spacecraft technology. `https://sst-soa.arc.nasa.gov` (2016). Accessed: 2019-05-16
20. Azur Space Solar Power GmbH, *30% Triple Junction GaAs Solar Cell Type: TJ Solar Cell 3G30C Advanced (80µm)* (2016)

21. R. Nader, et al., in *67th International Astronautical Congress* (2016)
22. Clyde Space, *User Manual: 3rd Generation EPS Range - No Inhibits* (2017). USM-1335 Rev. D
23. Innovative Solutions in Space. CubeSat deployers. `https://www.isispace.nl/wp-content/uploads/2016/02/ISIS-CubeSat-Deployers-Brochure-v1.pdf` (2016). Accessed: 2018-09-10
24. J.C. Liou, N.L. Johnson, N.M. Hill, Acta Astronautica **66**(5-6), 648 (2013). DOI 10.1016/j.actaastro.2009.08.005
25. C. Bonnal, J.M. Ruault, M.C. Desjean, Acta Astronautica **85**, 51 (2013). DOI 10.1016/j.actaastro.2012.11.009
26. C. Wiedemann, et al. Active debris removal, (2012). Paper DLRK 2012-281452
27. J.D. Seong, H.D. Kim, H.Y. Choi, Proceedings of the Institution of Mechanical Engineers, Part G: Journal of Aerospace Engineering **231**(1), 180 (2017). URL `10.1177/0954410016662065`
28. H. Sahara, Acta Astronautica **105**(1), 136 (2014). DOI 10.1016/j.actaastro.2014.08.026
29. N. Berend, X. Olive, Acta Astronautica **122**, 324 (2016). DOI 10.1016/j.actaastro.2016.02.005
30. H. Hakima, M.R. Emami, in *2017 IEEE Aerospace Conference* (2017), pp. 1–11. DOI 10.1109/AERO.2017.7943788
31. B.B. Virgili, H. Krag, in *5th Conference on Space Debris* (2009)
32. H. Hakima, M.R. Emami, in *9th International Conference on Recent Advances in Space Technologies (RAST)* (2019)
33. F. Aghili, Journal of Guidance, Control, and Dynamics **32**(5), 1671 (2009). DOI 10.2514/1.43189
34. R.H. Battin, *An Introduction to the Mathematics and Methods of Astrodynamics, Revised Edition* (American Institute of Aeronautics and Astronautics, 1999)
35. J.A. Kéchichian, *Applied Nonsingular Astrodynamics: Optimal Low-Thrust Orbit Transfer* (Cambridge University Press, 2018)